Supplementary Information

Origin of Structural Degradation in Li-rich Layered Oxide Cathode

Tongchao Liu[1,7], Jiajie Liu[2,7], Luxi Li[3,7], Lei Yu[4], Jiecheng Diao[5], Tao Zhou[4], Shunning Li[2], Alvin Dai[1], Wenguang Zhao[2], Yang Ren[3], Liguang Wang[3], Tianpin Wu[3], Rui Qi[2], Yinguo Xiao[2], Jiaxin Zheng[2], Wonsuk Cha[3], Ross Harder[3], Ian Robinson[5,6], Jianguo Wen[4], Jun Lu[1], Feng Pan[2*], Khalil Amine[1*]*

[1]*Chemical Sciences and Engineering Division, Argonne National Laboratory, Lemont, IL 60439, USA*
[2]*School of Advanced Materials, Peking University, Shenzhen Graduate School, Shenzhen 518055, China.*
[3]*X-ray Science Division, Argonne National Laboratory, Lemont, IL 60439, USA*
[4]*Center for Nanoscale Materials, Argonne National Laboratory, Lemont, IL 60439, USA*
[5]*London Centre for Nanotechnology, University College London, London WC1E 6BT, U.K.*
[6]*Condensed Matter Physics and Materials Science Department, Brookhaven National Laboratory, Upton, New York 11793, United States*

[7]*These authors contributed equally to this work.*

**Corresponding author: amine@anl.gov (K. A.); panfeng@pkusz.edu.cn (F. P.); junlu@anl.gov (J. L.);*

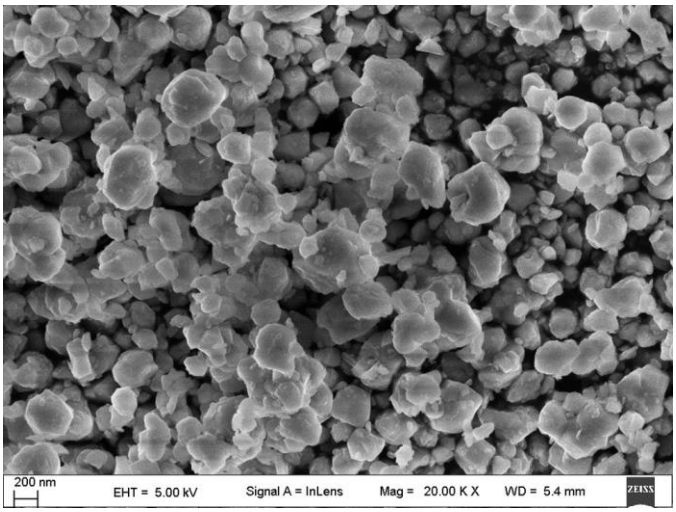

Supplementary Figure 1. The SEM image of the LMR powder. The particle size ranges from 300-600 nm, which is ideal for the BCDI measurement.

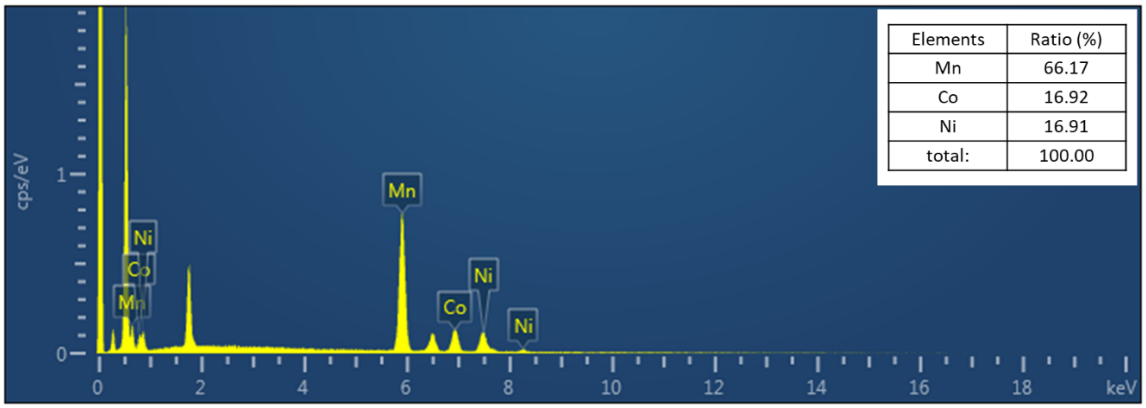

Elements	Ratio (%)
Mn	66.17
Co	16.92
Ni	16.91
total:	100.00

Supplementary Figure 2. SEM-EDS results of the pristine LMR cathode. The actual chemical composition complies well with the design (Mn : Co : Ni = 4 : 1 : 1).

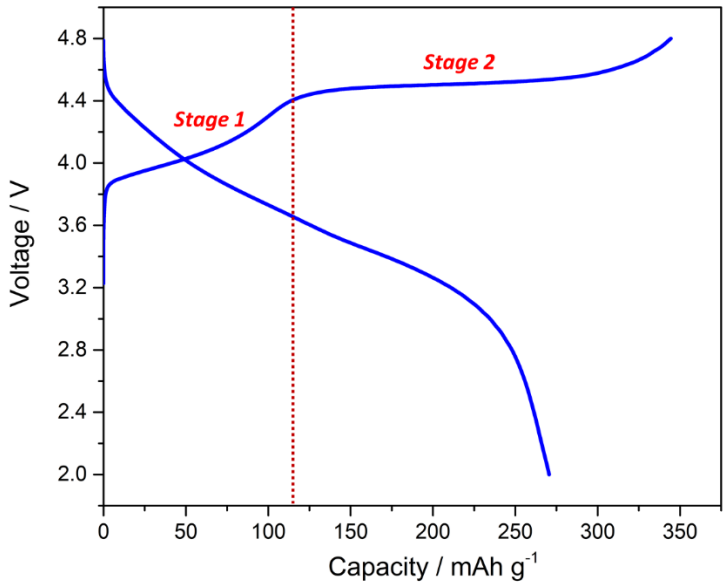

Supplementary Figure 3. The first charge/discharge curve of LMR cathode. The first charge profile exhibits two distinct electrochemical stages at different voltage ranges. Stage 1 corresponds to the oxidation of Ni and Co in $LiTMO_2$ domains. Stage 2 corresponds to the activation of Li_2MnO_3 domains.

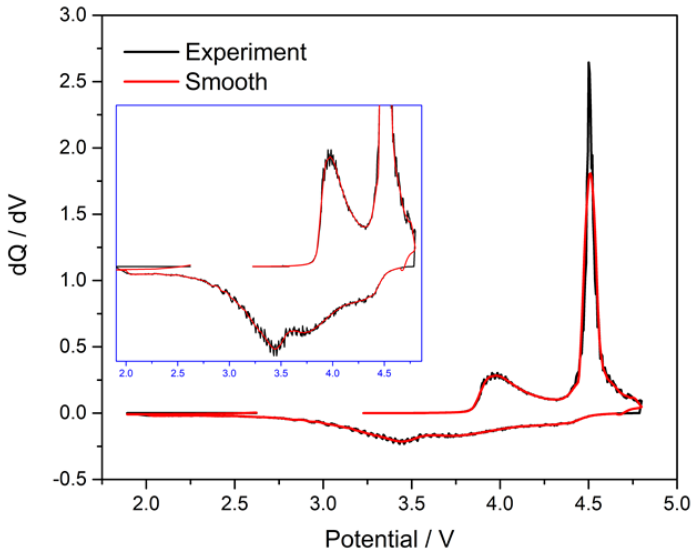

Supplementary Figure 4. The corresponding dQ/dV curve of the first charge/discharge curve. The dQ/dV curve of the first charge exhibits two oxidation peaks at different voltage ranges. The broad peak at 4.0 V corresponds to the oxidation of Ni and Co in $LiTMO_2$ domains. The sharp peak at 4.5 V corresponds to the activation of Li_2MnO_3 domains.

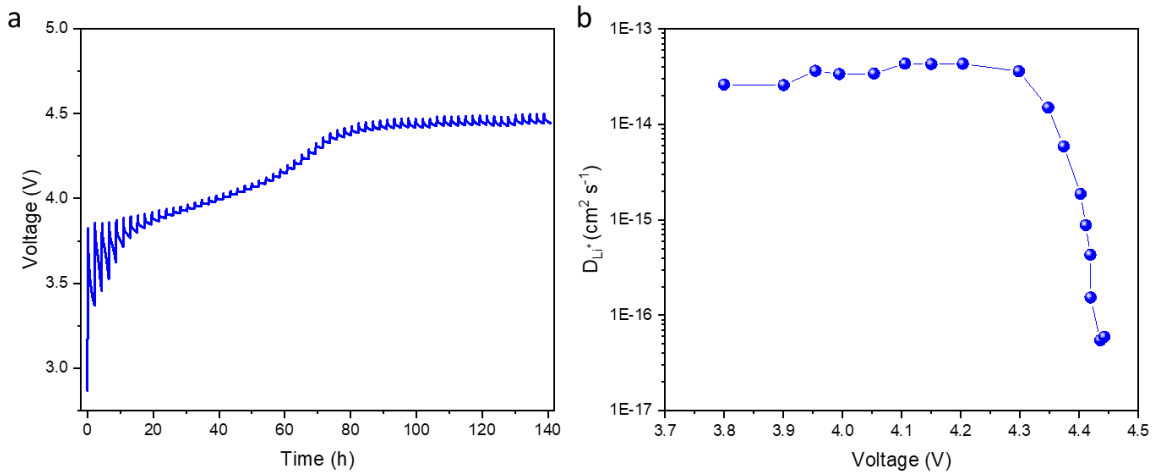

Supplementary Figure 5. The galvanostatic intermittent titration technique (GITT) test of the first charge. **a** The voltage profile derived from the GITT test. **b** Li ion diffusion coefficients during the first charge. The Li ion diffusion coefficient keeps stable in stage 1 but dramatically decreases after the activation of Li_2MnO_3 domains (stage 2).

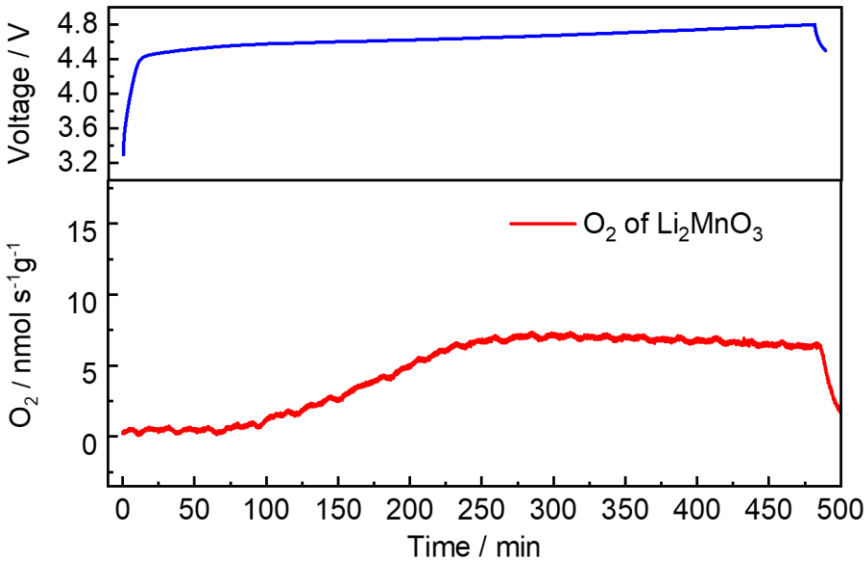

Supplementary Figure 6. *In-situ* differential electrochemical mass spectroscopy measurements for the first charge of Li_2MnO_3. The signal of O_2 evolution is not detected until 20% delithiation of Li_2MnO_3.

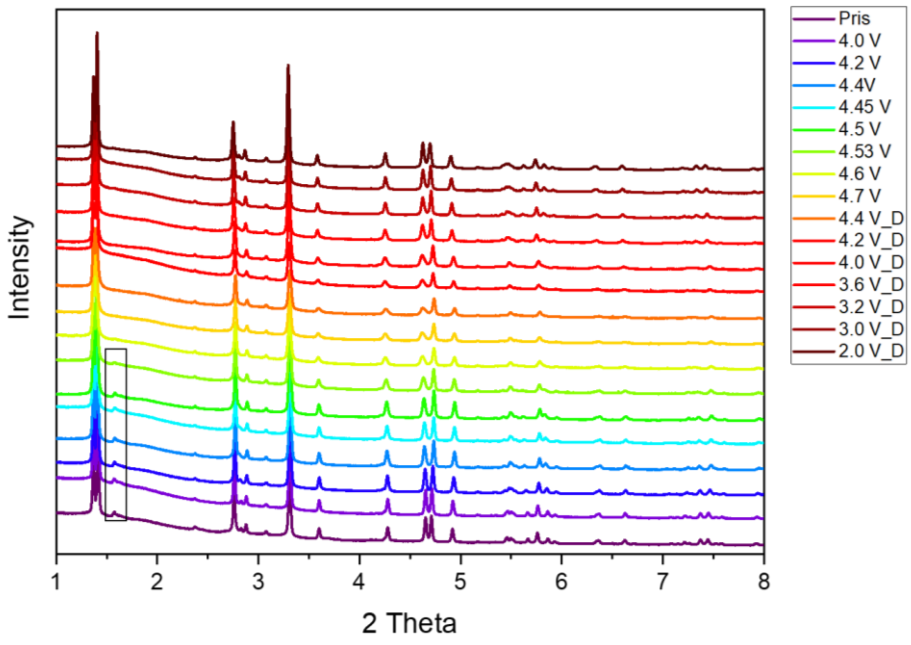

Supplementary Figure 7 The *ex-situ* XRD patterns of the first charge/discharge for the LMR cathode. The obvious lattice parameter changes can be observed from *ex-situ* XRD pattern, particularly in the 2 theta range of 3.0-6.0°.

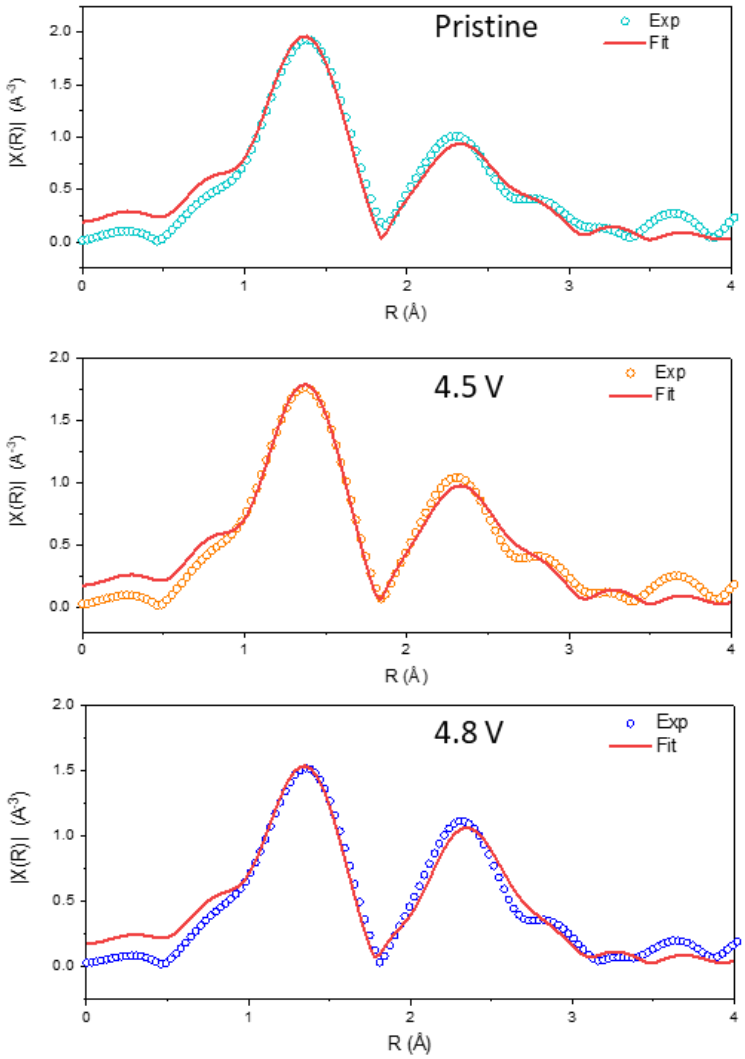

Supplementary Figure 8. *Ex-situ* Mn *K-edge* EXAFS spectra of the samples at pristine, 4.5V and 4.8V and the corresponding fitting results. Detailed fitting results are shown in Supplementary Table 2.

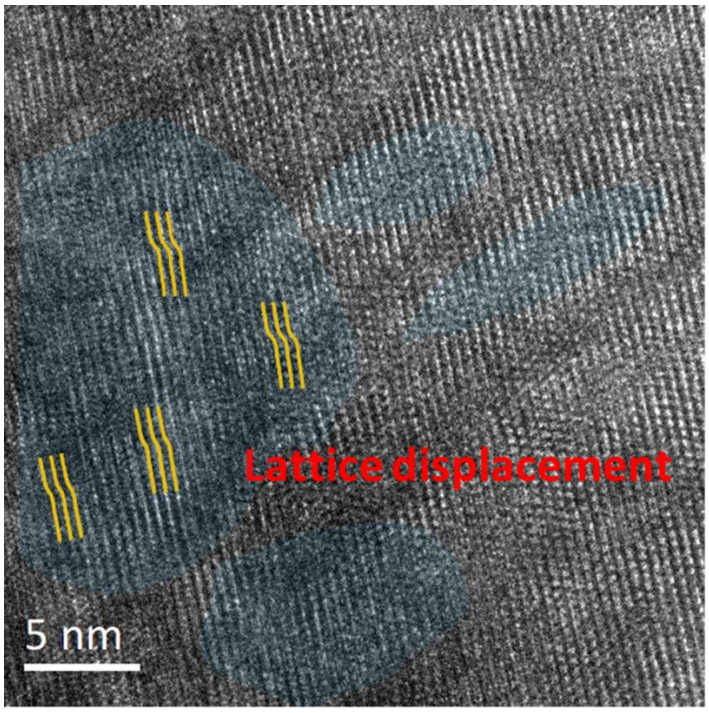

Supplementary Figure 9. Visible lattice displacement observations using TEM of the LMR charged to 4.47 V.

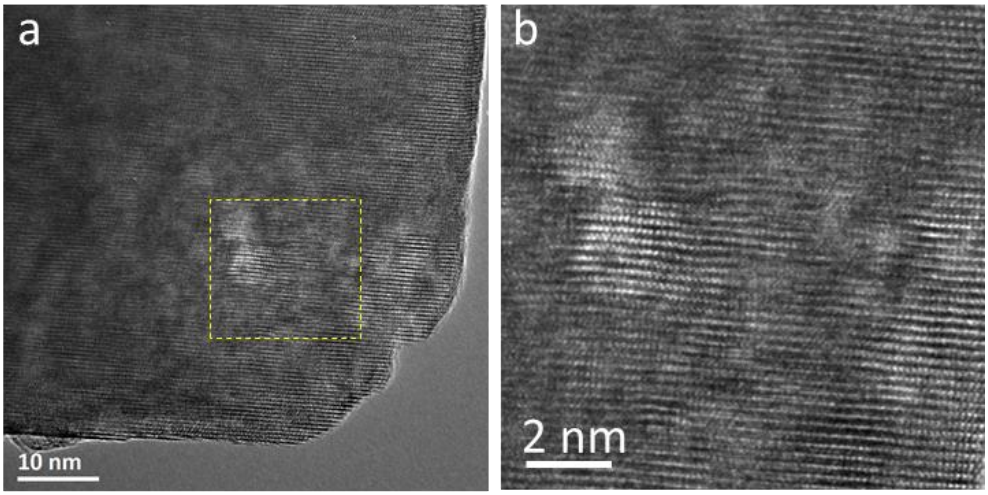

Supplementary Figure 10. Visible observations of the LMR charged to 4.5 V. **a.** High magnification TEM image of the LMR charged to 4.5 V. **b.** The enlarged image of the selected area in Supplementary Fig. 10a.

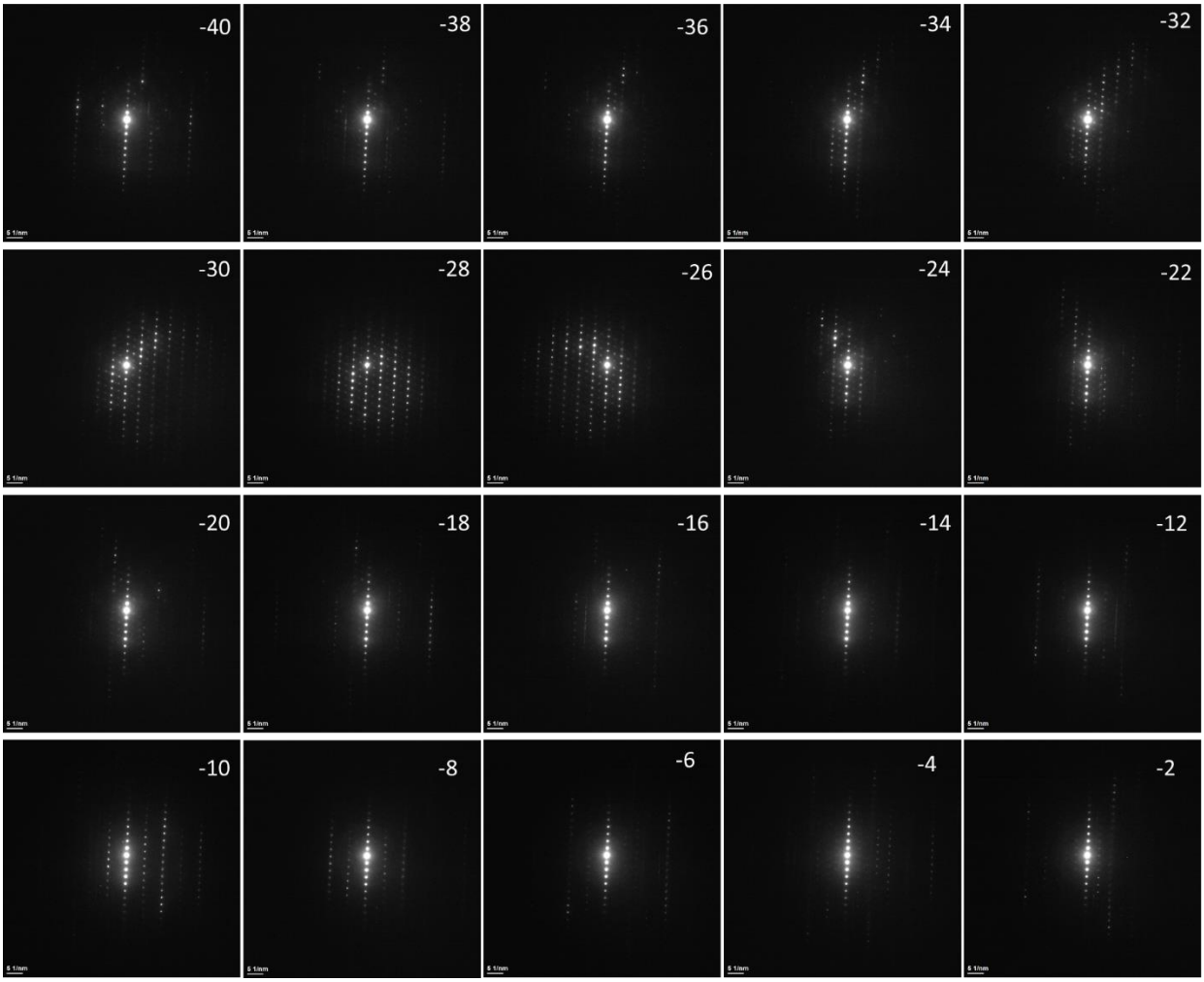

Supplementary Figure 11. The SEAD images captured at different rotation angles.

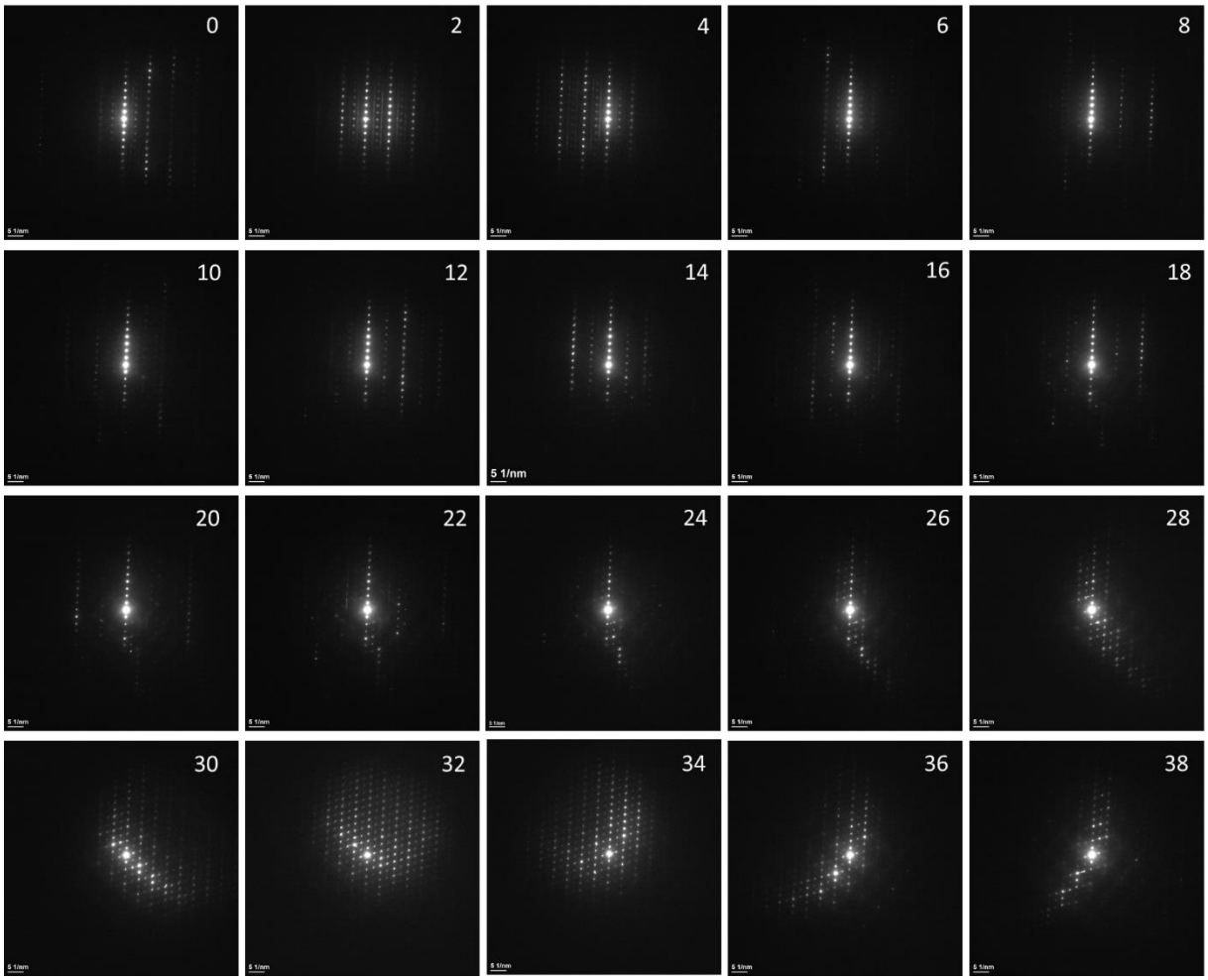

Supplementary Figure 12. The SEAD images captured at different rotation angles.

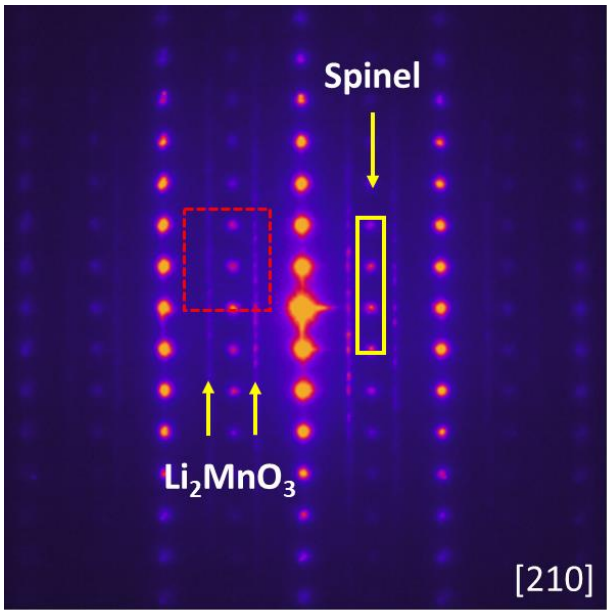

Supplementary Figure 13. The selected area electron diffraction (SAED) image of the sample charged to 4.5 V. In addition to the typical layered structure and weak Li_2MnO_3 reflection, the reflection that corresponds to the spinel lattice can be also observed.

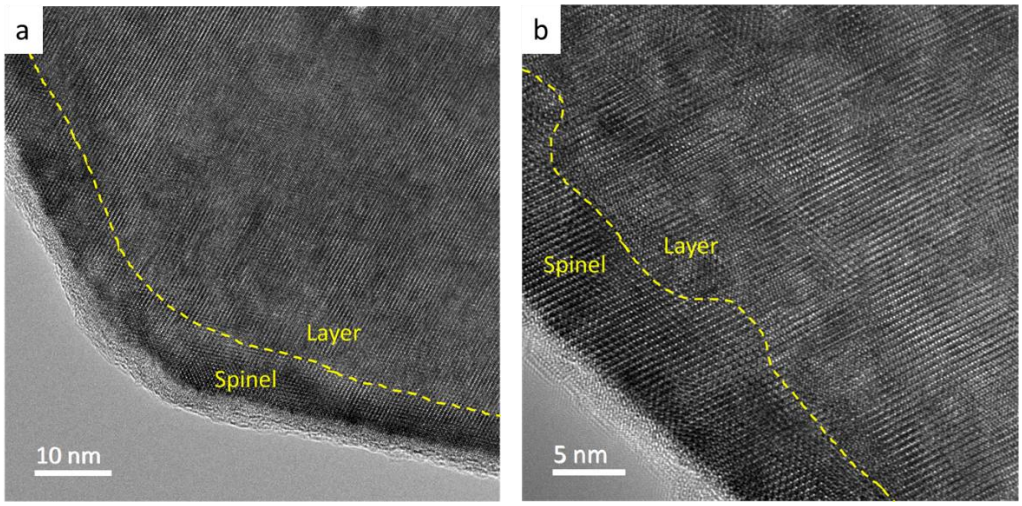

Supplementary Figure 14. Visible observations of the LMR charged to 4.8 V. **a** Low magnification TEM image of the LMR charged to 4.8 V. **b** High magnification TEM image of the LMR charged to 4.8 V. A clear reconstruction surface layer with the spinel phase can be visualized.

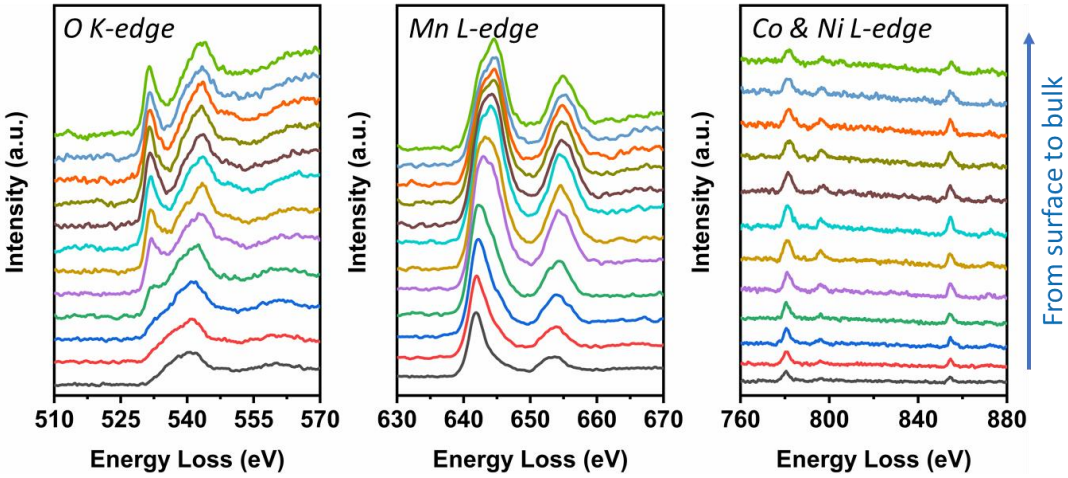

Supplementary Figure 15. Electron energy-loss spectroscopy line scans of the O *K-edge*, Mn *L-edge*, Co & Ni *L-edge* for the LMR charged to 4.8 V along the direction from surface to bulk. The intensity of O-K edge prepeaks substantially reduces from the interior to the exterior and almost disappears near the surface. Concurrently, Mn L-edge shows left shift near the surface.

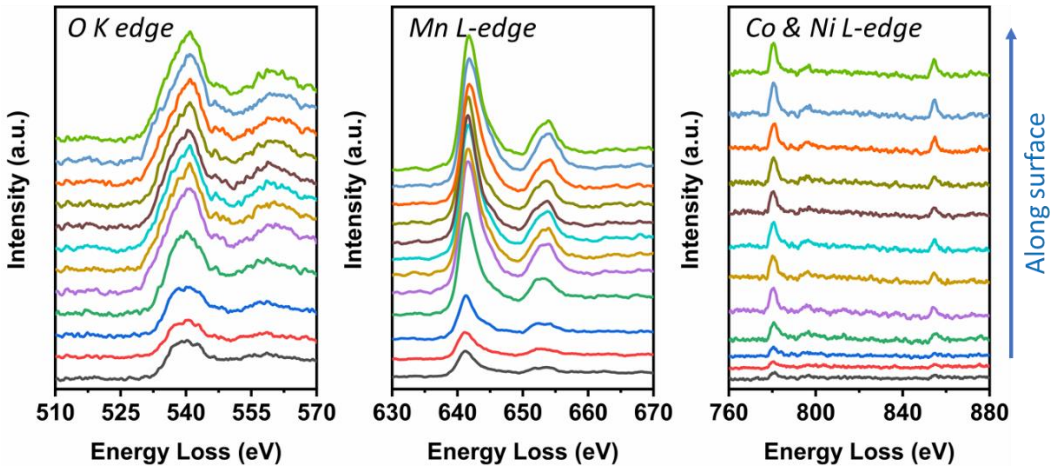

Supplementary Figure 16. Electron energy-loss spectroscopy line scans of the O *K-edge*, Mn *L-edge*, Co & Ni *L-edge* for the LMR charged to 4.8 V along the surface fringe. The O-K line-scan parallel to the surface confirms that the oxygen release uniformly occurs in the entire particle surface as the disappeared O prepeak.

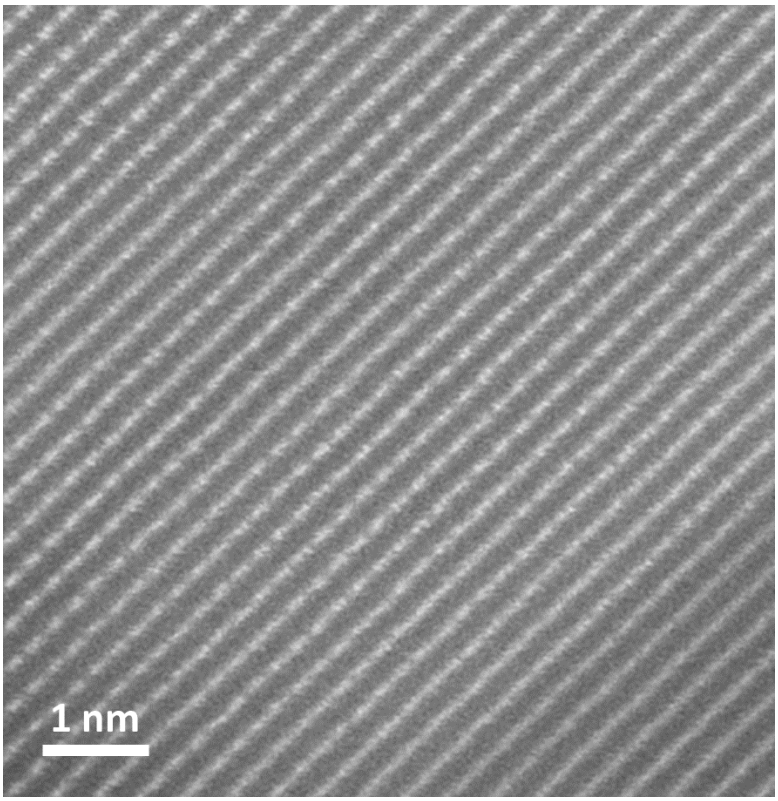

Supplementary Figure 17. High resolution TEM image showing the atomic arrangements of O2 phase LMR. The domain structure is eliminated and replaced by homogeneous atomic arrangement.

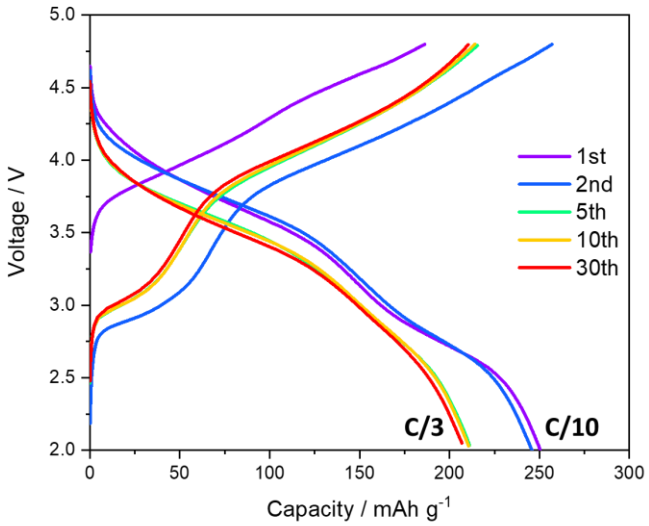

Supplementary Figure 18. The charge/discharge profiles of O2 phase based-LMR cathode. The cells were activated at C/10 within first 2 cycles and then cycled at C/3. The smooth charging behavior with no apparently differentiated voltage plateaus indicates effectively suppressed differential electrochemical activities.

Supplementary Table 1. Lattice parameters obtained by the two-phase structure model refinement of pristine LMR cathode.

Phases			
Phase 1 Space group: $R\bar{3}m$	**Phase fraction**		**0.57(4)**
	Lattice parameters	$a=b$	2.8535(6) (Å)
		c	14.2424(9) (Å)
		V	100.43(6) (Å^3)
Phase 2 Space group: $C2/m$	**Phase fraction**		**0.43(4)**
	Lattice parameters	a	4.9488(1) (Å)
		b	8.5485(4) (Å)
		c	5.0366(6) (Å)
		β	109.556(0) (°)
		V	200.78(2) (Å^3)
Agreement factors	Rwp (%)		5.73
	Rp (%)		5.86

Supplementary Table 2. Structural parameters of the samples obtained by fitting the EXAFS data. There are the average coordination number (CN), path distance (R), Debye-Waller factor (σ^2), threshold energy correction (ΔE), and the R-Factor of the fitting.

Samples	Shells	CN	R (Å)	σ^2 (Å^2)	ΔE (eV)	R-Factor
pristine	Mn-O	6	1.905	0.003	-5.3	0.014
	Mn-TM	2.8	2.869	0.003		
charged to 4.5 V	Mn-O	5.3	1.904	0.003	-4.7	0.010
	Mn-TM	2.7	2.873	0.003		
charged to 4.8 V	Mn-O	4.9	1.890	0.005	-7.7	0.015
	Mn-TM	3.8	2.875	0.005		